ChemComm

COMMUNICATION

View Article Online
View Journal

Cite this: DOI: 10.1039/c4cc04680c

Received 19th June 2014,
Accepted 28th July 2014

DOI: 10.1039/c4cc04680c

www.rsc.org/chemcomm

A hydrophobic hole transporting oligothiophene for planar perovskite solar cells with improved stability†

Lingling Zheng,[a] Yao-Hsien Chung,[a] Yingzhuang Ma,[a] Lipei Zhang,[a] Lixin Xiao,*[ab] Zhijian Chen,[ab] Shufeng Wang,[ab] Bo Qu[ab] and Qihuang Gong[a]

An oligothiophene derivative named DR3TBDTT with high hydrophobicity was synthesized and functioned as the hole transporting material without an ion additive. 8.8% of power conversion efficiency was obtained for $CH_3NH_3PbI_{3-x}Cl_x$ based planar solar cells with improved stability, compared to devices using Li-TFSI doped spiro-MeOTAD.

Recently, organic–inorganic hybrid perovskite materials have rapidly developed and attracted significant research interest due to their excellent absorption and transporting properties. $CH_3NH_3PbI_3$ and $CH_3NH_3PbBr_3$ were firstly used as the light absorbers in liquid dye-sensitized solar cells by Miyasaka *et al.*[1] Benefiting from the solid-state hole transporting material (HTM) of 2,2′,7,7′-tetrakis(*N*,*N*-di-*p*-methoxyphenylamine)-9,9′-spirobifluorene (spiro-MeOTAD), much higher power conversion efficiencies (PCEs) have been achieved in solid-state cells than those of liquid ones,[2–7] and exceeded 15% in a short term.[8–13] N. J. Jeon *et al.* changed *p*-OMe substituents of the conventional spiro-MeOTAD, 16.7% of PCE was obtained using the derivative with *o*-OMe substituents for meso-structured perovskite solar cells.[13] Owing to the difficulty in the purification of spiro-MeOTAD, many other triphenylamine derivatives were reported as the HTMs.[14–20] However, almost all these HTMs reported for solution-process perovskite solar cells needed the addition of ion additives, *e.g.*, lithium bis(trifluoromethylsulfonyl)imide (Li-TFSI) with 4-*tert*-butylpyridine (*t*BP) to achieve improved hole mobility and device performance.[13–27] Few HTMs in their pristine form can compete with additive doped spiro-MeOTAD for perovskite solar cells. P. Qin *et al.* reported a branched conjugated HTM working alone for *meso*-structured perovskite solar cells with a high PCE of 12.8%.[28] The use of Li-TFSI should be avoided, because it will not only increase the costs, but also seriously deteriorate the stability of the perovskite due to its high hydroscopicity leading to the decomposition of perovskite.[29,30]

Oligothiophenes containing a backbone structure of a benzodithiophene (BDT) unit as the central block and ethylrhodanine as the end group (DR3TBDTT) are highly efficient donors with a high hole mobility of 10^{-4} cm^2 V^{-1} s^{-1} in the bulk heterojunction solar cells.[31–33] In this article, we modified the alkyl groups of DR3TBDTT to obtain a low-lying energy level of the highest occupied molecular orbital (HOMO) (5.39 eV), matching with the HOMO of perovskite (5.43 eV) (Fig. 1). As a result, the highest PCE of 8.8% was achieved using DR3TBDTT adding a small amount of polydimethylsiloxane (PDMS) as the HTM without the ion additive, comparable to 8.9% for spiro-MeOTAD doped with Li-TFSI and *t*BP. Moreover, the resultant oligothiophene possessed a high hydrophobicity with a water contact angle of 107.4°, which can be expected to prevent water penetration. So, the perovskite in devices without the hydroscopic Li-TFSI showed improved stability resulting from the moisture resistance of oligothiophene. This work provides an alternative candidate for HTM dispensed with the ion additive for stable perovskite solar cells.

The solution and thin-film UV-vis absorption spectra of DR3TBDTT are presented in Fig. S1a.† DR3TBDTT in diluted

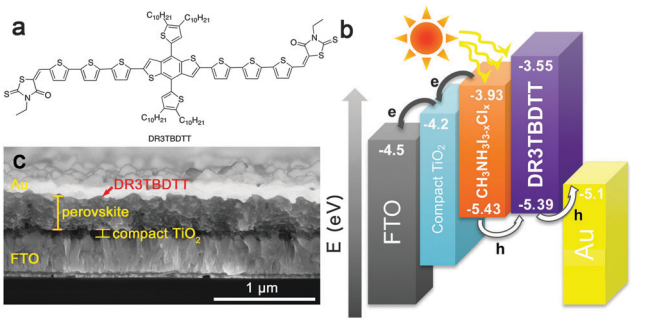

Fig. 1 (a) The chemical structure of DR3TBDTT. (b) The relative energy level diagram of a perovskite solar cell. (c) Cross-sectional SEM image of the planar perovskite solar cell using DR3TBDTT as the HTM.

[a] *State Key Laboratory for Mesoscopic Physics and Department of Physics, Peking University, Beijing 100871, China. E-mail: lxxiao@pku.edu.cn*

[b] *New Display Device and System Integration Collaborative Innovation Center of the West Coast of the Taiwan Strait, Fuzhou 350002, China*

† Electronic supplementary information (ESI) available: Experimental details; physical properties of DR3TBDTT; EDS; absorption spectra; stability of devices; repeatability of devices; device performance and EIS fitting results. See DOI: 10.1039/c4cc04680c

chloroform solution exhibited an absorption peak at 528 nm. The film spectrum showed two absorption peaks at 588 nm and 614 nm, one of which is a vibronic shoulder, corresponding to the π-orbital overlap between the molecule backbones.[31–33] The optical band gap was estimated to be 1.84 eV by the absorption onset of the film. The HOMO energy level was measured by photoelectron spectroscopy to be 5.39 eV (Fig. S2†), only 0.04 eV higher than the HOMO of $CH_3NH_3PbI_{3-x}Cl_x$, indicating an extremely low energy barrier for hole transporting. Density functional theory (DFT) calculations showed that the HOMO of DR3TBDTT was mainly located at the BDT unit, and its LUMO was mainly located at ethylrhodanine of both ends, revealing an acceptor–donor–acceptor (A–D–A) backbone structure (Fig. S1b†). The calculated HOMO energy level was 5.25 eV, close to the experimental result. Thermogravimetric analysis (TGA) and differential scanning calorimetry (DSC) analysis showed excellent stability of DR3TBDTT, with a high melting point of 224 °C and decomposition temperature of 398 °C (Fig. S3†).

To test the performance of DR3TBDTT, planar perovskite solar cells based on the structure of FTO/compact TiO_2/$CH_3NH_3PbI_{3-x}Cl_x$/HTM/Au were fabricated (Fig. 1). A 350 nm thick $CH_3NH_3PbI_{3-x}Cl_x$ layer was fabricated by sequential deposition, using a mixture of PbI_2–$PbCl_2$ as the precursor according to our previous report.[34,35] The HTM layers were deposited by spin-coating. Besides using DR3TBDTT alone, we blended it with a widely-used flow agent of PDMS to improve the morphology.[31,32,36] The influences of the conventional additive Li-TFSI and *t*BP on the performance and stability were also studied.

The scanning electron microscope (SEM) images were employed to observe the morphology of the HTM on the perovskite layer (Fig. 2). All the relative elements can be observed in the respective energy dispersive spectra (EDS) (Fig. S4†). From a solution of DR3TBDTT, the perovskite layer was only partially covered by HTM, probably due to the much larger surface tension of the solution than the surface energy of the perovskite,[36] which made it extremely difficult to form a continuous and uniform film on the perovskite layer with a roughness of tens of nanometers.[4,35] With the aid of 0.1 mg ml^{-1} PDMS, full coverage on the highly textured surface of perovskite was obtained, since the difference of the surface tension and the defects of the film could be eliminated by its low surface tension and high viscosity.[36] The introduction of Li-TFSI and *t*BP into DR3TBDTT solution led to a decreased coverage, appearing as the smaller domains of HTM on the perovskite. The HTM-coated perovskite films showed additional absorption at 500–670 nm consistent with the absorption of DR3TBDTT, and slightly higher absorption for the film containing PDMS in this region also indicated more adhesion of HTM as shown in the SEM images (Fig. S5†).

80 nm thick Au was thermally evaporated under vacuum on the HTM as the cathode. As a comparison, devices containing widely used spiro-MeOTAD + Li + *t*BP as the HTM were also fabricated. The performance of each device under 100 mW cm^{-2} simulated AM1.5G irradiation are shown in Fig. 3a and listed in Table S1.† The PCE of the device with DR3TBDTT as HTM was 4.9%, with a low short-circuit current (J_{sc}) of 12.6 mA cm^{-2} and a low fill factor (FF) of 0.42. By using DR3TBDTT + PDMS as the HTM, the performance improved significantly with a PCE of 8.8%, a J_{sc} of 15.3 mA cm^{-2}, a FF of 0.60 and an open circuit voltage (V_{oc}) of 0.95 V, comparable to 8.9% PCE for spiro-MeOTAD + Li + *t*BP based devices with a V_{oc} of 0.93 V. A higher V_{oc} of DR3TBDTT + PDMS devices attributed to the deeper HOMO energy level (5.39 eV) of DR3TBDTT than that of spiro-MeOTAD (5.22 eV).[14] But the very close HOMO between

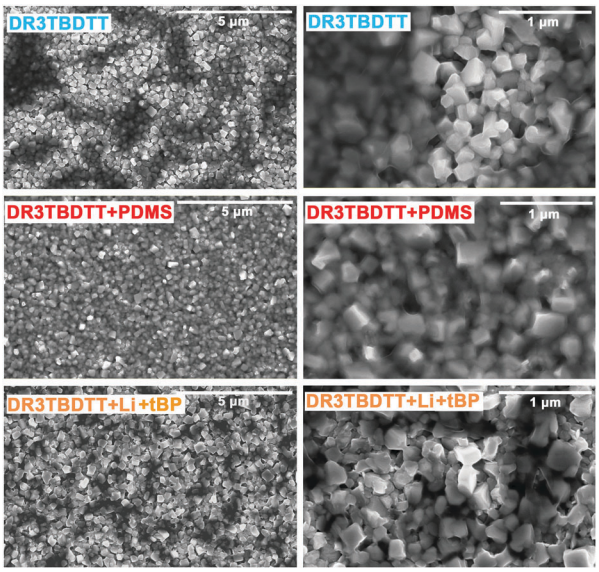

Fig. 2 Top-view SEM images of perovskite layers covered by DR3TBDTT based HTMs (scale bar = 5 μm and 1 μm).

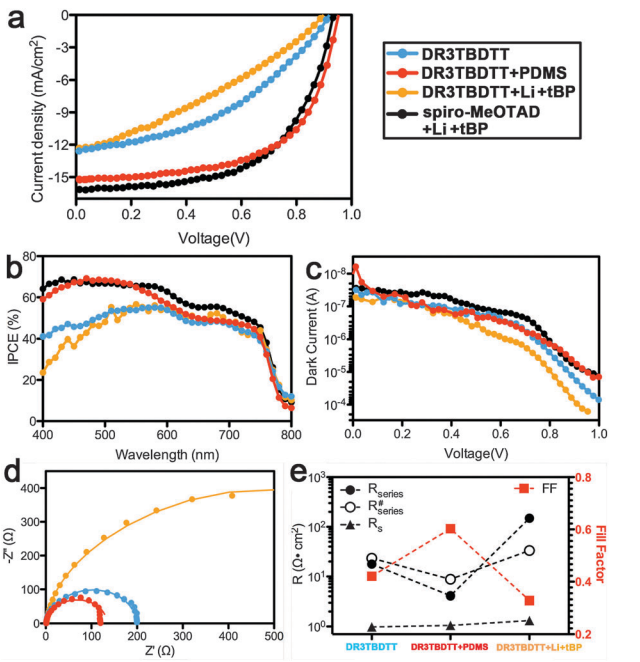

Fig. 3 (a) *J*–*V* curves, (b) IPCE, and (c) the dark current of the planar perovskite solar cells with different HTMs. (d) Nyquist plots and the fitting line of perovskite solar cells in the perovskite/Au interface under the dark at respective V_{oc}. (e) R_s and R_{series} obtained from EIS analysis compared to $R^{\#}_{series}$ and FF deduced from the *J*–*V* curves.

DR3TBDTT and perovskite is unfavorably for charge transfer, resulting in the lower J_{sc}. Devices with DR3TBDTT + Li + *t*BP showed the poorest performance, especially of V_{oc} and FF. As shown in Fig. 3c, at higher forward bias, the dark current increased from DR3TBDTT + PDMS to DR3TBDTT and to DR3TBDTT + Li + *t*BP based devices, illustrating increased recombination leading to decreased V_{oc}.[37,38] As a result, the 0.17 eV HOMO level shift was not reflected in the extra V_{oc} for the devices based on DR3TBDTT and DR3TBDTT + Li + *t*BP. The incident photon to current conversion efficiency (IPCE) (Fig. 3b) showed the same shapes for all devices, suggesting that the absorption of the very thin DR3TBDTT has a negligible effect on the solar cells.[14,15] The integrated J_{sc} calculated from the IPCE are well matched with the J_{sc} from *J*–*V* curves.

Electrochemical impedance spectra (EIS) were employed to explain the significant difference of FF and the relations with the morphology of the HTM. The high-intermediate frequency arcs are shown in Fig. 3d, representing two individual processes, corresponding to the charge-transport resistance of the Au/HTM interface and overlapping partially with the resistance in the HTM.[37–41] We fitted the high frequency feature with a parallel *R*–*C* circuit. The series resistance (R_s) can be obtained from the intersections of these arcs, corresponding to the resistance of the conducting glass, contacts and wires. The fitted resistance (R_{pc}) from the arcs mostly attributed to the resistance at the Au/HTM interface, because the HTM formed very thin overlayers (Fig. S6†) in this study and its resistance is too small to resolve.[37] Therefore, the total series resistance of the devices can be calculated as $R_{series} = R_s + R_{pc}$, which has a serious effect on FF (Table S1†). As a consequence, DR3TBDTT + Li + *t*BP based devices with the largest R_{series} have the lowest FF, and DR3TBDTT + PDMS based devices achieved the highest FF of 0.60 with the smallest R_{series} of only 4.1 Ω cm^2. The R_{series} calculated from EIS matched the series resistance calculated from the *J*–*V* curve ($R^{\#}_{series}$) well and had a contrary tendency of FF (Fig. 3e). A large interface resistance was derived from the partial bareness of the perovskite, leading to a direct contact of perovskite and Au.[38] A full coverage of HTM on the perovskite layer is advantageous to fabricate an efficient device with a high FF. Therefore, an optimized hole transporting layer (HTL) should be a continuous, uniform film with the minimum thickness on top of the perovskite, consistent with the conclusions made by A. Dualeh *et al.*[37]

Li-TFSI in our study failed to enhance device performances, likely stemmed from two effects. Firstly, the introduction of Li-TFSI accompanying with its polar solvent into the solution of DR3TBDTT led to a reduced coverage on the perovskite resulting in low FF and PCE. Secondly, the thickness of HTL using conventional spiro-MeOTAD in devices usually needs to reach more than 140 nm, so the ion salt is essential to assist the hole transporting in such a thick film due to the poor pristine mobility of spiro-MeOTAD.[23,26,37] In our case, the thin capping layer of DR3TBDTT with higher hole mobility as its analog as reported[31,32] does not need the ion additive.

To define the role of PDMS, a device exclusively using PDMS to replace the HTM was fabricated and the performance of such a device was as poor as the device without any HTM (Fig. S7†). Moreover, DR3TBDTT with a higher content of PDMS exhibited an abnormal *J*–*V* curve demonstrating a huge resistance in the device derived from the excess addition of insulated PDMS. Besides, the XRD results revealed no obvious difference of molecule packing between the DR3TBDTT film and the DR3TBDTT + PDMS film (Fig. S8†). To sum up, the role of insulated PDMS was limited as a flow agent, which assisted the formation of a continuous, uniform and thin HTL, resulting in a significant enhancement of device performance.

All the devices exhibited good stabilities when stored under a relatively low humidity of ~20% (Fig. S9†). After 13 days of aging, the PCEs of spiro-MeOTAD + Li + *t*BP and DR3TBDTT + Li + *t*BP based devices decreased from 8.3% to 7.7% and 3.3% to 3.1%, respectively, with a ~6% reduction relative to the initial PCEs. While the performance decreased slightly from 8.3% to 8.1% for DR3TBDTT + PDMS based devices (~2% reduction) and did not decline for DR3TBDTT based devices. However, when the devices of different HTMs were stored in a high relative humidity of above 50%, the differences of device stability can be observed obviously (Fig. 4a). Perovskite in devices containing Li-TFSI totally decomposed from dark brown to yellow after 3 days, with a sharp decline of PCE from 3.7% to 0.9% and 8.9% to 3.7% for DR3TBDTT + Li + *t*BP and spiro-MeOTAD + Li + *t*BP based devices, respectively (Fig. S10†). On the other hand, the perovskite in devices using DR3TBDTT and DR3TBDTT + PDMS still appeared dark brown, with the PCE changing from 4.9% to 4.4% and 8.8% to 8.0%, respectively, representing a superior stability. The obvious difference of device stability resulted from greatly different hydrophobicity of the HTL (Fig. 4b). DR3TBDTT films showed a very big water contact angle of 107.4°, so that the hydrophobic HTLs can efficiently prevent the water penetration into the perovskite layer.[21] With the addition of PDMS, the angle declined slightly to 99.5°, still much bigger than that of spiro-MeOTAD + Li + *t*BP films. Both films containing Li-TFSI showed the smaller water contact angle of around 80°, revealing an increased affinity of water caused by Li-TFSI. Such hydroscopic ion additives should be avoided in practical applications for perovskite solar cells due to their negative influence on device stability.

In summary, the hole transporting material DR3TBDTT was successfully synthesized with a well-matched HOMO energy level of 5.39 eV and excellent hydrophobicity for planar perovskite solar cells. By the addition of PDMS, a continuous thin capping layer on

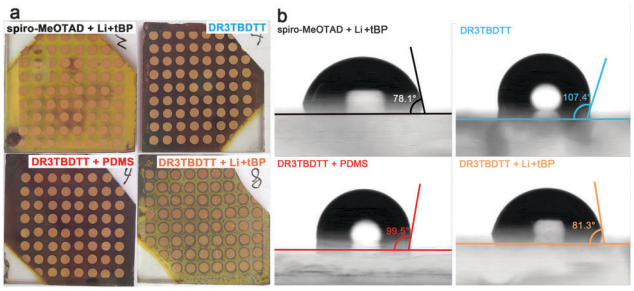

Fig. 4 (a) Devices exposed to a relative humidity >50% in air for 3 days at room temperature without encapsulation under illumination. (b) Water contact angles of each HTM films on a glass substrate.

perovskite was formed as the HTL. The highest PCE for devices using DR3TBDTT + PDMS as the HTM reached 8.8% without the addition of Li-TFSI, comparable to 8.9% obtained from spiro-MeOTAD + Li + *t*BP. However, the introduction of Li-TFSI into the HTMs led to decreased device stability due to the hydroscopicity of the ion additives. HTL composed of hydrophobic DR3TBDTT can efficiently protect the perovskite layer from moisture, so that the devices exhibited excellent stability. This work provides an efficient candidate of ion additive-free HTMs for highly stable perovskite solar cells.

We acknowledge the financial support from the National Natural Science Foundation of China (61177020 and 11121091) and the National Basic Research Program of China (2013CB328700). The authors are thankful to Mr Xiao Yu and Prof. Dechun Zou of the College of Chemistry and Molecular Engineering of Peking University for their kind help in the assistance in the electrochemical impedance measurements.

Notes and references

1 A. Kojima, K. Teshima, Y. Shirai and T. Miyasaka, *J. Am. Chem. Soc.*, 2009, **131**, 6050.
2 H.-S. Kim, C.-R. Lee, J.-H. Im, K.-B. Lee, T. Moehl, A. Marchioro, S.-J. Moon, R. Humphry-Baker, J.-H. Yum, J. E. Moser, M. Grätzel and N.-G. Park, *Sci. Rep.*, 2012, **2**, 591.
3 M. M. Lee, J. Teuscher, T. Miyasaka, T. N. Murakami and H. J. Snaith, *Science*, 2012, **338**, 643.
4 Q. Chen, H. Zhou, Z. Hong, S. Luo, H.-S. Duan, H.-H. Wang, Y. Liu, G. Li and Y. Yang, *J. Am. Chem. Soc.*, 2014, **136**, 622.
5 N. Pellet, P. Gao, G. Gregori, T.-Y. Yang, M. K. Nazeeruddin, J. Maier and M. Grätzel, *Angew. Chem., Int. Ed.*, 2014, **53**, 3151–3157.
6 H.-S. Kim, S. H. Im and N.-G. Park, *J. Phys. Chem. C*, 2014, **118**, 5615.
7 H. J. Snaith, *J. Phys. Chem. Lett.*, 2013, **4**, 3623.
8 J. Burschka, N. Pellet, S.-J. Moon, R. Humphry-Baker, P. Gao, M. K. Nazeeruddin and M. Grätzel, *Nature*, 2013, **499**, 316.
9 D. Liu and T. L. Kelly, *Nat. Photonics*, 2014, **8**, 133.
10 J. T. Wang, J. M. Ball, E. M. Barea, A. Abate, J. A. Alexander-Webber, J. Huang, M. Saliba, I. Mora-Sero, J. Bisquert, H. J. Snaith and R. J. Nicholas, *Nano Lett.*, 2014, **14**, 724.
11 K. Wojciechowski, M. Saliba, T. Leijtens, A. Abate and H. J. Snaith, *Energy Environ. Sci.*, 2014, **7**, 1142.
12 M. Liu, M. B. Johnston and H. J. Snaith, *Nature*, 2013, **501**, 395.
13 N. J. Jeon, H. G. Lee, Y. C. Kim, J. Seo, J. H. Noh, J. Lee and S. I. Seok, *J. Am. Chem. Soc.*, 2014, **136**, 7837.
14 A. Krishna, D. Sabba, H. Li, J. Yin, P. P. Boix, C. Soci, S. G. Mhaisalkar and A. C. Grimsdale, *Chem. Sci.*, 2014, **5**, 2702.
15 T. Krishnamoothy, F. Kunwu, P. P. Boix, H. Li, T. M. Koh, W. L. Leong, S. Powar, A. Grimsdale, M. Gräztel, N. Mathews and S. G. Mhaisalkar, *J. Mater. Chem. A*, 2014, **2**, 6305.
16 H. Li, K. Fu, A. Hagfeldt, M. Gräztel, S. G. Mhaisalkar and A. C. Grimsdale, *Angew. Chem., Int. Ed.*, 2014, **53**, 4085.
17 N. J. Jeon, J. Lee, J. H. Noh, M. K. Nazeeruddin, M. Gräztel and S. I. Seok, *J. Am. Chem. Soc.*, 2013, **135**, 19087.
18 J. Wang, S. Wang, X. Li, L. Zhu, Q. Meng, Y. Xiao and D. Li, *Chem. Commun.*, 2014, **50**, 5829.
19 S. Lv, L. Han, J. Xiao, L. Zhu, J. Shi, H. Wei, Y. Xu, J. Dong, X. Xu, D. Li, S. Wang, Y. Luo, Q. Meng and X. Li, *Chem. Commun.*, 2014, **50**, 6931.
20 J. H. Heo, S. H. Im, J. H. Noh, T. N. Mandal, C.-S. Lim, J. A. Chang, Y. H. Lee, H.-j. Kim, A. Sarkar, M. K. Nazeeruddin, M. Gräztel and S. I. Seok, *Nat. Photonics*, 2013, **7**, 486.
21 Y. S. Kwon, J. Lim, H.-J. Yun, Y.-H. Kim and T. Park, *Energy Environ. Sci.*, 2014, **7**, 1454.
22 H. Chen, X. Pan, W. Liu, M. Cai, D. Kou, Z. Huo, X. Fang and S. Dai, *Chem. Commun.*, 2013, **49**, 7277.
23 H. J. Snaith and M. Gräztel, *Adv. Mater.*, 2007, **19**, 3643.
24 U. B. Cappel, T. Daeneke and U. Bach, *Nano Lett.*, 2012, **12**, 4925.
25 R. Schölin, M. H. Karlsson, S. K. Eriksson, H. Siegbahn, E. M. J. Johansson and H. Rensmo, *J. Phys. Chem. C*, 2012, **116**, 26300.
26 A. Abate, T. Leijtens, S. Pathak, J. Teuscher, R. Avolio, M. E. Errico, J. Kirkpatrik, J. M. Ball, P. Docampo, I. McPherson and H. J. Snaith, *Phys. Chem. Chem. Phys.*, 2013, **15**, 2572.
27 R. Katoh, M. Kasuya, S. Kodate, A. Furube, N. Fuke and N. Koide, *J. Phys. Chem. C*, 2009, **113**, 20738.
28 P. Qin, S. Paek, M. I. Dar, N. Pellet, J. Ko, M. Gräztel and M. K. Nazeeruddin, *J. Am. Chem. Soc.*, 2014, **136**, 8516.
29 J. H. Noh, S. H. Im, J. H. Heo, T. N. Mandal and S. I. Seok, *Nano Lett.*, 2013, **13**, 1764.
30 G. Niu, W. Li, F. Meng, L. Wang, H. Dong and Y. Qiu, *J. Mater. Chem. A*, 2014, **2**, 705.
31 J. Zhou, Y. Zuo, X. Wan, G. Long, Q. Zhang, W. Ni, Y. Liu, Z. Li, G. He, C. Li, B. Kan, M. Li and Y. Chen, *J. Am. Chem. Soc.*, 2013, **135**, 8484.
32 J. Zhou, X. Wan, Y. Liu, Y. Zuo, Z. Li, G. He, G. Long, W. Ni, C. Li, X. Su and Y. Chen, *J. Am. Chem. Soc.*, 2012, **134**, 16345.
33 Y. Liu, Y. Yang, C.-C. Chen, Q. Chen, L. Dou, Z. Hong, G. Li and Y. Yang, *Adv. Mater.*, 2013, **25**, 4657.
34 Y. Ma, L. Zheng, Y.-H. Chung, S. Chu, L. Xiao, Z. Chen, S. Wang, B. Qu, Q. Gong, Z. Wu and X. Hou, *Chem. Commun*, 2014, DOI: 10.1039/C4CC01962H.
35 L. Zheng, Y. Ma, S. Chu, S. Wang, B. Qu, L. Xiao, Z. Chen, Q. Gong, Z. Wu and X. Hou, *Nanoscale*, 2014, **6**, 8171.
36 J. W. Du, in *Coatings Technology Handbook*, ed. A. A. Tracton, CRC Press, Boca Raton, FL, USA, 3rd edn, 2006, ch. 75.
37 A. Dualeh, T. Moehl, N. Tétreault, J. Teuscher, P. Gao, M. K. Nazeeruddin and M. Gräztel, *ACS Nano*, 2014, **8**, 362.
38 E. J. Juarez-Perez, M. Wußler, F. Fabregat-Santiago, K. Lakus-Wollny, E. Mankel, T. Mayer, W. Jaegermann and I. Mora-Sero, *J. Phys. Chem. Lett.*, 2014, **5**, 680.
39 V. Gonzalez-Pedro, E. J. Juarez-Perez, W.-S. Arsyad, E. M. Barea, F. Fabregat-Santiago, I. Mora-Sero and J. Bisquert, *Nano Lett.*, 2014, **14**, 888.
40 H.-S. Kim, I. Mora-Sero, V. Gonzalez-Pedro, F. Fabregat-Santiago, E. J. Juarez-Perez, N.-G. Park and J. Bisquert, *Nat. Commun.*, 2013, **4**, 2242.
41 Y. Xu, J. Shi, S. Lv, L. Zhu, J. Dong, H. Wu, Y. Xiao, Y. Luo, S. Wang, D. Li, X. Li and Q. Meng, *ACS Appl. Mater. Interfaces*, 2014, **6**, 5651.

